Experimental study on the effectiveness of strengthening over-deformed segmental tunnel lining by steel plates

Zhai, Wuzhou; Chapman, David; Zhang, Dong-ming; Huang, Hong-wei

DOI:
10.1016/j.tust.2020.103530

Document Version
Peer reviewed version

Citation for published version (Harvard):
Zhai, W, Chapman, D, Zhang, D & Huang, H 2020, 'Experimental study on the effectiveness of strengthening over-deformed segmental tunnel lining by steel plates', *Tunnelling and Underground Space Technology*, vol. 104, 103530. https://doi.org/10.1016/j.tust.2020.103530

Experimental study on the effectiveness of strengthening over-deformed segmental tunnel lining by steel plates

Wuzhou Zhai[1,2], David Chapman[2], Dongming Zhang[1]*, Hongwei Huang[1]

[1] Department of Geotechnical Engineering, College of Civil Engineering, Tongji University, Shanghai, China.

[2] School of Civil Engineering, College of Engineering and Physical Sciences, University of Birmingham, Birmingham, UK.

* Corresponding author, Email: 09zhang@tongji.edu.cn

Abstract: The method of using steel plates to strengthen existing tunnel linings has been widely applied in many tunnel rehabilitation projects around the world. However, the effectiveness of the strengthening resulting from this method is still unclear, especially for conditions when the segmental linings are deformed to a relatively large extent. In this paper, a series of physical model tests conducted in 1-g plane strain conditions were designed to study the strengthening effectiveness of steel plates for over-deformed segmental tunnel linings. The results show that the segmental tunnel linings affected by the ground surface surcharge will deform nonlinearly, as the complex behaviour of the segment joints at different positions lead to a gradual degradation of the tunnel overall performance. Once the deformed segmental tunnel linings were strengthened by steel plates, the stiffness and capacity of the tunnel were improved by 190% and 69%, respectively, compared to those without strengthening. Subsequently, the strengthening effectiveness of tunnels strengthened at different deformation stages are compared quantitatively. It is found that an increase in the tunnel deformation before strengthening led to a decrease in the stiffness and an increase in the total capacity of the tunnel after strengthening, while the increased capacity was

less affected.

Keywords: Segmental tunnel lining, Steel plate strengthening, Model test

1. Introduction

Shield-driven tunnels play an important role in the development of urban underground infrastructure systems. Once constructed, these tunnels are usually expected to last for a hundred years. However, due to unpredictable changes in the surrounding environment and the constructed characteristics of segmental linings themselves, the tunnels can face high risks of being disturbed or even damaged by potential accidents throughout their lives. Accidents related to operating tunnels being adversely affected by external disturbances are often reported from time to time, for example from adjacent excavations (Chang et al., 2001a), from piling constructions (RAIB, 2014), from ground surface surcharge (Huang et al., 2016), and from flooding (Van Empel et al., 2006). The affected segmental linings were severely damaged in these accidents, which threatened the safety of the tunnel systems. Therefore, effective rehabilitation measures for damaged tunnels after such events are important to guarantee their continued safety during the future service.

There are several ways to strengthen damaged tunnel linings, amongst which the steel plates strengthening method has been widely adopted due to its various advantages (Chang et al., 2001b, Kiriyama et al., 2005, Shao et al., 2016). The main phases of this method can be summarized as: First, the steel plates sections are manufactured according to the inner profile of the tunnel that needs to be strengthened; Second, the steel plate sections are installed and welded to form an inner steel ring connected to the existing tunnel linings; Third, the gap between the new steel plate linings and the original concrete segmental linings is filled with mortar or epoxy resin to ensure that

44 the two components behave as a composite lining system. In this way, the increasing lining
45 deformation is controlled and the capacity of tunnel structure can be enhanced.
46 Although this strengthening method has been widely applied to repair tunnels in soft soils, there is
47 always a question on when is the optimal time to conduct the strengthening treatment of a deformed
48 tunnel. It is obvious that the time determines not only the safety of tunnel lining structure, but also
49 the cost of the whole tunnel repair project. Therefore, it is essential to understand the influence of
50 existing degree of damage on the post-strengthening tunnel performance, as only then will the most
51 appropriate time for strengthening be determined.
52 There has been some research focusing on tunnel strengthening using steel plate linings. Liu et al.
53 (2017) performed a full-scaled structural test on a segmental lining ring strengthened by steel plates.
54 In this experiment, a real RC (reinforced concrete) segmental ring was strengthened by additional
55 bonded steel plate linings, and 24 hydraulic jacks were utilized to apply a system of point loads to
56 simulate the soil pressure. The steel plates were installed inside the deformed segmental lining ring
57 with the load being applied, and then the strengthened tunnel was loaded continuously until failure
58 occurred. The test result demonstrated the effectiveness and failure mode of this strengthening
59 method, and some parametric analyses were conducted by Zhao et al. (2016) using a new
60 simplified numerical approach. However, using jacking loads neglects the important soil-structure
61 interaction, and the high demand in terms of cost, space and equipment of such a full-scale
62 experimental approach make it hard to repeat and conducted for other arrangements. Zhang et al.
63 (2019a) presented a numerical study of steel plate strengthened segmental tunnel linings using FE
64 (finite element) tools, where the soil-structure interaction and the tunnel-steel interface were
65 appropriately simulated. However, the influence of the structural damage before strengthening, and

66 the phenomenon of strengthening failure was difficult to simulate due to limitations with the
67 numerical techniques.
68 Therefore, further studies are required to better understand this tunnel strengthening method. In
69 the field of geotechnical engineering, physical model tests have always been a useful and
70 fundamental way to study sophisticated geo-structure problems (Wood, 2014). Compared with full-
71 scaled testing, small-scaled model tests have advantageous for following reasons: (1) they can be
72 performed with better control on the model details, (2) they allow the information about the expected
73 patterns of response to be obtained more rapidly, (3) they can be performed repeatedly at relative
74 low cost. Generally, laboratory tests for buried tunnels can be performed either under natural (single)
75 gravity conditions (1-g) (Kojima and Yashiro, 2005, Chapman et al., 2006, Zhang et al., 2015) or in
76 a centrifuge, which applies multiple gravities to be applied in a test (Mair et al., 1993, Meguid et al.,
77 2008, Kiani et al., 2016). In this research, a 1-g model test was designed and performed to study
78 the steel plates strengthening method for segmental tunnel linings, so that: (1) the operation of the
79 steel plates strengthening can be performed manually during test, which could not be easily
80 achieved in a centrifuge environment; (2) the tunnel models required relatively larger scale ratio in
81 this research to reveal detailed patterns of segmental tunnel lining behaviours with and without
82 steel plates strengthening, which would have been difficult to conduct in an ordinary centrifuge.
83 In this paper, a scaled physical model tests for segmental tunnel linings strengthened by steel
84 plates performed in 1-g plane strain conditions are described. The techniques for modelling of soil,
85 concrete segments, segmental joints and steel plates strengthening are introduced in sequence.
86 The effectiveness of the steel plate strengthening are demonstrated by comparing the results
87 obtained from the tests for tunnels with and without strengthening. Subsequently, the behaviour of

the tunnel strengthened at different deformation stages are summarised and analysed to show the influence of the degree of deformation on the post-strengthening lining performance.

2. Physical model test

2.1. Prototype

As reported by Huang et al. (2016), hundreds of rings of segmental tunnel linings with an outer diameter of 6.2m of Shanghai Metro Line 2 were severely disrupted due to an unexpected surface surcharge, where a maximum transverse lining deformation in term of horizontal convergence ratio reached 35.7‰. During the tunnel repair process, steel plate linings were adopted to strengthen the damaged tunnel sections. This tunnel and related ground conditions have been used as the prototype in this research. Detailed information on this tunnel strengthening project can be found from previous literature (Zhao et al., 2016, Zhang et al., 2019b).

The scaling law (Wood, 2014) has been applied to set up the relationship between the prototype and the model. The scale factor for length n_l was first determined as 1:15, based on the soil tank dimensions. In the 1-g experiment condition, since sand is utilized to model ground soil, the scale factor for its unit weight n_γ is determined as 1:1. Therefore, the scale factors for other quantities were determined by using dimensional analysis as shown in Table 1. It should be noted that the listed scale ratios are the ideal values which were difficult to achieve perfectly. Therefore, some compromises had to be adopted when making decisions related to the tunnel and soil model materials, which will be explained in the following paragraphs.

2.2. Experimental apparatus

A soil tank with a size of 2m high, 2m wide and 0.4m thick was used for the experiments. As shown in Fig. 1 and Fig. 2, the soil tank has rigid side walls with a smooth inner surface made from ceramic. There are two square-shaped openings with a size of 0.8m×0.8m at the middle of the walls covered by 40 mm thick transparent Perspex plates. On one side, there is a circular opening with a radius of 175mm in the Perspex plate, allow access for the strengthening operation and installation of the sensors and wires. On the other side, a camera was placed focusing on the tunnel to capture the deformation profiles of the deforming tunnel. A jack with a rigid plate footing was placed on the top soil surface to provide surcharge load on the ground surface during the experiment. The tunnel lining deformation was measured by four 40mm-LVDT (linear variable differential transfer) devices placed at positions of the tunnel crown, invert and spring-line. Circumferential strains on both the inner and outer surfaces of the lining segments were measured by RSG (resistance strain gauge) every 45°around the tunnel section.

2.3. Modelling of the soils

A true model can be obtained only when governing laws for all qualities are satisfied. However, for 1-g model tests associated with geotechnical problems, it is necessary to make things achievable with an adequate model, which maintains a “first order” similarity (Harris and Sabnis, 1999). Since large transverse tunnel deformations were measured in actual case mentioned before, observable lining deformation was required in the 1-g model tests, which closely related to the compressibility of the model soil. Therefore, a mass of rubber particles with good compression characteristics was used to model the soil layer near the tunnel, while dry medium sand was used for the rest of the

ground soil to provide gravity stresses (as shown in Fig. 2). The soil material is placed and tamped in layers 20cm thick so that the tank was filled to as similar degree of homogeneity and density as possible for all the tests.

The model soil materials are shown in Fig. 3. Their physical properties and grain characteristics were tested and the corresponding parameters are listed in Table 2. In addition, compressibility tests and direct shear tests were conducted on both materials to capture their mechanical properties, and the results are shown in Fig. 4. The compression modulus of rubber particles is determined as 0.51MPa, considering the scale ratio in Table 1, and the corresponding compression modulus of prototype soil was 7.65MPa. The prototype soil layers in which the real tunnels were constructed are layers ③-⑤ Shanghai silty clay, and this material has the compression modulus varying between 1.32~11.5 MPa (Huang et al., 2016). Therefore, the rubber particles are appropriated for use as the model soil in this experiment.

2.4. Modelling of the segmental tunnel linings

One of the main challenges for the model test in this research was how to model the segmental tunnel linings properly. It is acknowledged that the existence of joints is definitely the most vital structural characteristic for segmental linings of shield-driven tunnels (Do et al., 2013). To date, there are two main modelling strategies for segmental tunnel linings. One approach is using model segments made of solid materials (e.g. metal, Perspex), which are easy to be cut into segments from a tube so that they can then be assembled as rings (Lee and Ge, 2001, Ye et al., 2014, Standing and Lau, 2017, Zheng et al., 2017). Using this approach, the joint behaviour can be modeled appropriately, but the influence of fragility property and cracks are ignored. The second

149 approach is to cast a whole tunnel lining using a mortar material (e.g. cement mortar, gypsum
150 mortar) using a specific mould (Zhang et al., 2015, Wang et al., 2019b). In this way, the segmental
151 joints are usually modelled by grooves at appropriate positions. The advantage of this approach is
152 that the mortar casting materials are similar to concrete, which can simulate the lining cracking and
153 crushing behaviour while being stressed. However, since the discontinuous rotations between
154 adjacent segments at the joints are the main cause of the large transverse deformation of
155 segmental tunnel linings in soft soils (Huang et al., 2016), the continuous lining rings with simply a
156 reduction in thickness at the joint positions can't reflect either the complex joint behaviour or the
157 lining overall deforming pattern. In addition, the failure of steel plates strengthened tunnels always
158 occurs as a thin layer of the lining concrete at the interface being pulled off (Liu et al., 2017).
159 Therefore, the tunnel model material with a mechanical characteristic similar to concrete is
160 important to achieve modelling of the strengthening failure mode. A tunnel model considering both
161 casting and joint characteristics is proposed and applied in this research.
162 The tunnel model was designed as shown in Fig. 5 and 6 with the dimensions listed in Table 3. The
163 tunnel model was made of gypsum mortar, iron wire and iron pieces. There were two iron pieces
164 placed at every position of the segmental joint, and the wires were circled through the iron pieces
165 with the aim of modelling the bolt connection of the joints, as seen in Fig.6 (b). Based on the study
166 of Wang et al. (2019a), the gypsum mortar mix using water, gypsum and diatomite in a proportion
167 of 1:1.3:0.1 was selected to meet the scale ratio required in this research. The mechanical
168 parameters of the lining gypsum were measured using uniaxial compression tests. The parameters
169 are listed in Table 4.
170 When the overall deformation of the segmental tunnel linings occurs as shown in Fig. 7, segments

171 rotate relative to the adjacent ones at the joints. In this way, the wire will be placed in tension and
172 behave as bolts. Therefore, the stiffness of the iron wires is a key parameter which considerably
173 influences both the joint stiffness and overall stiffness of a lining ring. In this research, the
174 requirement of wire size is to keep overall stiffness of the model tunnel similar to that of the
175 prototype. The effective ratio of the transverse bending rigidity (η) is often adopted as a general
176 index to evaluate the overall stiffness of segmental rings during the design process for segmental
177 tunnel linings (Lee and Ge, 2001, Koyama, 2003). Based on the study of the segmental tunnel
178 linings in the Shanghai metro, Huang et al. (2006) suggested that the value of η equals 0.67 for the
179 straight-jointed assembly conditions. This value is adopted to determine the size of the wire for the
180 tunnel model in this research. A finite element model for the tunnel model was developed by using
181 FE software ABAQUS as shown in Fig. 6 (a), which is assembled using lining segments simulated
182 by solid elements and embedded iron wires simulated by beam elements. The material properties
183 were assumed to be elastic and given the properties listed in Table 3. By applying the same
184 concentrated load at the tunnel crown in the numerical models, the vertical diameter changes of
185 the continuous ring ($\Delta D_{v,CR}$) and segmental linings ($\Delta D_{v,SL}$) could be obtained as shown in Fig. 6
186 (b). The value of η was evaluated as $\eta = \frac{\Delta D_{v,CR}}{\Delta D_{v,SL}}$. Thus, the η values of model tunnels with different
187 iron wire sizes could be calculated numerically, from which the wires with a Φ1.6mm were adopted
188 in this research.
189 The manufacture process use for the tunnel model is shown in Fig. 8. An assembled mould is
190 designed and used for producing the tunnel models. Following these six steps, an appropriate
191 model for the segmental tunnel linings was obtained as shown in the “Step 6” in Fig. 8.
192 There are four lining rings in one test. Ideally, all the segmental lining rings should behave identically

in the plane strain test condition. The adjacent lining rings were designed to be connected using screws and wire. As shown in Fig. 6 (a), the screws were installed every 45° around the lining external profile in the tunnel transverse section. Fig. 6 (b) presents a detailed drawing of the connection, with wire used to secure the adjacent screws on the adjacent lining rings. Thus, eight sets of such connection pairs were constructed along the tunnel section to secure one lining ring to another.

2.5. Modelling the steel plate strengthening for existing tunnels

Aluminum plates were employed to model the steel plates for strengthening the tunnel linings. The aluminum plate size was determined using the scaling law by following equation:

$$I_m = n_{EI} \cdot \frac{E_p}{E_m} I_p \quad (1)$$

Where n_{EI} is the scale ratio for the flexural rigidity listed in Table 1, E_p and E_m are the elastic modulus of the prototype and the model, $I = bt^3/12$ is the rotation inertia of the aluminum or steel plate sections, b and t are the width and thickness of the steel or aluminum plates. In this research, $E_p = E_s = 200GPa$, $E_m = E_a = 70GPa$, $b_p = 1000mm$, $t_p = 30mm$. Thus, the appropriate size of the aluminum plates section was adopted as $b_m = 60mm$, $t_m = 1.2mm$.

The process of steel plate strengthening in the model tests is illustrated in Fig. 9. First, the epoxy resin glue was uniformly smeared onto the inner surface of segmental tunnel linings. Subsequently, the aluminum plates with a length of the half inner tunnel circumference were installed at corresponding positions one after another, which were fixed to tunnel lining with screws (shown as Fig. 9 (a)). With all the aluminum plates installed, the whole strengthening was finally completed after 24 hours to allow the epoxy resin glue to set. The strengthening process was thus completed

and the strengthened segmental tunnel lining is shown in Fig. 9 (b). The purpose of using screws was to fix the steel plates position during the curing of the epoxy resin adhesive, although the screws themselves would have enhanced the interface property.

2.6. Tests procedure

During all the tests, the surcharge load was applied at intervals of 0.75kN to the soil surface in the test tank. Additional load was not applied until the movement of the loading plate stopped, thus, the whole loading process could be considered static. Tests for the strengthened tunnels were conducted in three steps as shown in Fig. 10. In Step 1, the applied load P was increased to p_1, in which the tunnel without steel plates (noted: in the model test were aluminum plates) was stressed to a deformed status. In Step 2, the applied p_1 was unloaded to model an unloading process. The deformed tunnel was then strengthened with the steel plates. In Step 3, another surcharge load $P=p_3$ was applied onto the strengthened tunnel. This step was not stopped until failure occurred in the strengthened lining.

A series of tests for tunnels strengthened at different degrees of deformation are listed in Table 5. Test No.1 is for the segmental tunnel lining without any strengthening treatment, while Tests No.2 to No.4 are for tunnels strengthened by steel plates. The surcharge load before strengthening (p_1) is varied to stress the tunnels to different degrees of deformation before strengthening.

3. Results and data analysis

In this section, the experimental data will be analysed with respect to the model scale. The analysis for tunnels without strengthening (Test No. 1) will be presented in Section 3.1. The analysis for

234 tunnels with steel plate strengthening (Test No. 2) will be presented later.

235 ***3.1. Tunnel without strengthening (Test No. 1)***

236 The test No. 1 was conducted on a tunnel without strengthening. The tunnel profiles before and
237 after loading are shown in Fig. 11 (a) and (b), where the overall shape of tunnel changed from a
238 circle to an oval as the applied load increased. It was observed that the tunnel crown went
239 downwards and the lining expanded horizontally at the spring-line. The relative deformation
240 increased at larger rate as the surcharge increased. Joint opening was observed during the test,
241 with the joints near the tunnel crown opening inwards, while the joints near the tunnel spring-line
242 opening outwards. A creak broke through the lining segment near the tunnel invert at end of the
243 test.

244 The changing values in the horizontal and vertical diameters of the tunnel lining are presented in
245 terms of P-ΔD curves in Fig. 12. The tunnel deformation developed nonlinearly as the load being
246 increased. When P<2kN, both ΔD_h and ΔD_v increased slightly and equally, which means the tunnel
247 linings were still deforming as a circular shape with good structural conditions. When 2kN<P<5kN,
248 ΔD_h and ΔD_v increased by 4-6mm, which indicate that the tunnel gradually deformed from a circle
249 to an oval shape. Changes in curve slopes implies a decrease in the overall lining stiffness. When
250 P>5kN, ΔD_h and ΔD_v developed rapidly, with a small increase in the applied load resulting in a
251 significant change in the tunnel lining profile.

252 From the measured tunnel deformation, significant loss of tunnel lining stiffness was observed
253 when the tunnel profile changed from a circle to an oval shape. This overall stiffness loss was a
254 result of some of the partial defects within the lining segments. Some of the detailed features within

255 the damaged segmental tunnel linings are shown in Fig. 13. Inward openings of the joints near the
256 tunnel crown were observed as shown in Fig. 13 (a), where relative rotation occurred between
257 adjacent segments resulting in the segment outer edges being compressed. In contrast, outward
258 openings were observed at the joints near the tunnel spring-line as shown in Fig. 13 (b), where
259 relative rotation occurred resulting in the segment inner edges being compressed to crush due to
260 stress concentration (Fig. 13 (c)). As illustrated in Fig. 13 (d), at positions near the tunnel invert,
261 cracks arose and developed through the invert segment from the inner to the outer edges, which
262 resulted in a significant reduction in bending rigidity of these segments. Therefore, it was a result
263 of all these partial defects that led to a reduction in the overall stiffness degradation of the segmental
264 tunnel linings.
265 The circumferential strain values were measured at the inner and outer tunnel surfaces by attached
266 strain gauges. The strain development at locations of the tunnel crown, spring-line and invert are
267 illustrated in Fig. 14, respectively.
268 The strains at the tunnel crown are shown in Fig. 14 (a), and demonstrate there was compression
269 on the outer edge and tension on the inner edge, which indicates a bending moment leading to the
270 inward joint opening near the tunnel crown (as seen in Fig. 13 (a)). The absolute values of both the
271 tension and compression strains increased as the applied load increased, while the magnitudes in
272 compression were higher than those in tension.
273 The lining conditions at the tunnel spring-line are shown in Fig. 14 (b), an demonstrate there was
274 tension on the outer surface and compression on the inner surface, which indicates a bending
275 moment leading to outward joints openings near the tunnel spring-line (as seen in Fig. 13 (b)). The
276 magnitudes of the inner compressive strains were higher than those of outer surface tensile strains.

277 The strains at the tunnel invert are shown in Fig. 14 (c), and demonstrate there was compression
278 on the outer surface and tension on the inner surface.
279 A sudden drop in tensile strains at the tunnel invert was observed at P=5.2kN (Fig. 14 (c)), which
280 is just at the moment that the crack within segment D occurred, seen in Fig. 13 (d). The appearance
281 of the cracks at the tunnel invert resulted in a sudden reduction in bending rigidity of segment D,
282 which led to stress relief at the invert and simultaneous stress intensity elsewhere (seen as a
283 sudden change in the strain values in Fig. 14 (a) and (b) at P=5.2kN). This redistribution of stress
284 was also accompanied with an increase in overall deformation and reduction in integral structural
285 stiffness observed as an inflection in the P-ΔD curves in Fig. 12.

286 ***3.2. Tunnel strengthened by steel plates (Test No. 2)***

287 Subsequent to the results of the tunnel without strengthening (Test No. 1), Test No. 2 involved the
288 over-deformed tunnel being strengthened by steel plates (modelled by aluminum plates).
289 Photographs of the tunnel at moments just after strengthening and then just after strengthening
290 failure are shown in Fig. 15 (a) and (b) respectively. In Fig. 15 (a), the tunnel profile had already
291 deformed to an oval shape, with defects such as joint openings and cracks visible. This deformed
292 tunnel was then strengthened using the aluminum plates as described in Section 2.5.
293 During the loading process after strengthening, no significant additional deformation in the
294 strengthened tunnel lining was observed until a sudden failure occurred at the interface between
295 the tunnel lining and the aluminum plates accompanied with a sound of breaking. A sudden
296 movement of segment linings was observed with a downwards movement at the tunnel crown and
297 outwards movement at the tunnel spring-line. The final profile after the strengthening failure is

298 shown in Fig. 15 (b), where severe damage of tunnel lining and a significant debonding at tunnel-
299 steel interface can be observed. In contrast, the tunnel without steel plates deformed gradually
300 without a sudden failure as the surcharge load increased (as seen in Fig. 11).
301 Some details of the strengthened tunnel after the occurrence of strengthening failure are shown in
302 Fig. 16. Debonding failure occurred at the interface between the tunnel lining and the steel plate in
303 the ranges 20~50° and 200~230° (clockwise from the tunnel crown), where a thin layer of gypsum
304 attached to aluminum plates was detached from the segment surface. A significant shear crack
305 throughout the segment was observed near tunnel crown where the debonding failure occurs, this
306 is because the sudden interface failure resulted in a sharp increase in the shear force within the
307 lining segment. It should be noted that, the interface conditions at the positions near the tunnel
308 spring-line were still well-bonded.
309 The evolution of the tunnel deformation before and after the installation of the steel plate can be
310 illustrated as P-ΔD_h and P-ΔD_v curves as shown in Fig. 17 (a) and (b). When P<6kN, the trends of
311 both the P-ΔD_h and P-ΔD_v curves coincide well with the curves for the tunnel without strengthening.
312 Subsequently, as the tunnel was unloaded at P=6kN, the horizontal tunnel diameter recovered by
313 0.7mm (as shown in Fig. 17 (a)), and the vertical tunnel diameter expanded by approximate 0.2mm
314 (as shown in Fig. 17 (b)).
315 The damaged tunnel was strengthened at a deformation of ΔD_h =9.3mm and ΔD_v =11.8mm. As
316 observed in Fig. 17, the behaviour after strengthening demonstrates the structural stiffness of the
317 strengthened lining was significantly improved by 1.9 times compared to that of the tunnel without
318 strengthening. The deformation of the strengthened segmental lining didn't change much until the
319 debonding failure occurred at P=11.7kN, and the bearing capacity is improved by 69%. As

mentioned previously, the brittle debonding failure at the interface resulted in an abrupt loss in structural stiffness of the strengthened tunnel lining, after which the tunnel lining behaved flexibly and the applied surcharge load could not be increased.

The strains of the lining segments and the steel plates were measured at different positions as shown in Fig. 18. Due to the strengthening operation in the tunnel during the experiment, strain gauges could only be attached to the outer surface of the lining segments and the aluminum plate. The strains measured at the tunnel crown are illustrated in Fig. 18 (a). The outer surface of the lining segment was compressed, while the aluminum plates were in tension. It can be seen that the segment strain reduced to zero without any residual strain after the unloading at P=6kN. After strengthening, the tensile strain in the aluminum plates and the compression strain in the outer surface of the tunnel increased simultaneously as the surcharge load increased until the sudden strengthening failure occurrd at P=11.7kN. The strain in aluminum plate instantaneously reduced at this point due to the interface debonding failure near tunnel crown, after which the aluminum plates near the tunnel crown were no longer stressed.

The strains measured at the tunnel spring-line are illustrated in Fig. 18 (b). The lining segment was subjected to tension on the outer surface, while the aluminum plate was subjected to compression. There was still some residual strain evident within the segments at this position after the unloading at P=6kN. After strengthening, the compressive strain in the aluminum plate and the tensile strain in the lining segment kept increasing until failure occurred.

The strains measured at the tunnel invert are illustrated in Fig. 18 (c). It is observed that there was only a small proportion of strain recovered after the unloading.

From strain measurements at all three positions when the strengthening failure happened at

342 P=11.7kN, it can be observed in Fig. 18 (a) and (c) that there was a sharp decline in tensile strains
343 of the steel plate at the tunnel crown and invert. This is because of the sudden interface debonding
344 failure near the tunnel crown and invert, as seen in Fig. 18. Thereafter, the strengthened aluminum
345 plates no longer behaved as a component of the composite lining system. This explains the reason
346 for the sudden drop in overall structural stiffness in the tunnel lining observed in Fig. 17.
347 To investigate how the steel plates behave when used to strengthen the existing segmental tunnel
348 linings, the strain values measured at different loading stages (P=2kN, 6kN and 10kN) are
349 presented in Fig. 19, where tensile strains are positive and compressive strains are negative. It is
350 observed that the aluminum plate was subjected to compression at 90° and 270°, while it is in
351 tension at other measurement positions. All the strains increased as the load P being increased.
352 The maximum tensile strain appeared at the tunnel invert and the maximum compressive strain
353 appeared at the tunnel spring-line, while the absolute value of the maximum tension strain is nearly
354 twice as high compared to the maximum compressive strain.

355 **4. Discussion**

356 As introduced in Section 2.6, tunnels being strengthened at different degrees of damage were
357 tested, i.e. Test No. 2 is the tunnel being strengthened at (P_1=6kN, ΔD_{h1}=9mm, ΔD_{v1}=11mm), Test
358 No. 3 is the tunnel being strengthened at (P_1=4kN, ΔD_{h1}=3mm, ΔD_{v1}=5mm), and Test No. 4 is the
359 tunnel being strengthened at (P_1=0, ΔD_{h1}=0, ΔD_{v1}=0). In this section, the performance of tunnels in
360 all these tests are compared in terms of the load-deformation curves to show the influence of the
361 existing deformation on post-strengthened tunnel performance.
362 For the comparison purpose, two dimensionless indicators, i.e. ovality and surcharge level, are

363 proposed as Equations (2) and (3) to evaluate the changes in tunnel transverse profiles and the
364 degree of the applied surcharge load, respectively.

365 $$O = \left(\Delta D_h + \Delta D_v \right) / 2D_0 \quad (2)$$

366 $$SL = p / \gamma h \quad (3)$$

367 where ΔD_h and ΔD_v are absolute values of the changing in horizontal and vertical tunnel diameters,
368 p is the equivalent surcharge calculated as applied load P divided by the square of the soil box
369 cross section, γ and h are the unit weight of sand and cover depth of the tunnel shown in Table 2.
370 The behaviour of the strengthened tunnels in the different tests are illustrated as the *SL*-*O* curves
371 as shown in Fig. 20. To emphasise the improvement in the lining performance due to the
372 strengthening, only the parts of curves exceeding the curve for the tunnel without strengthening
373 are kept in this figure.
374 In order to quantitatively compare the improvement of the tunnel stiffness due to strengthening, a
375 linear regression for the data of the *SL*-*O* curves from the starting point of the strengthening to the
376 failure point of the strengthening are presented in Fig. 20. The regression coefficients have been
377 used to define a stiffness improvement ratio (denoted by k_s), since this value indicates the
378 composite tunnel stiffness of the segmental lining after strengthening.
379 As seen in Fig. 20, the stiffness improvement ratio $k_{s\text{-}4}$ for test No.4 equals 1.37 ($k_{s\text{-}3}$=1.12 for test
380 No.3, $k_{s\text{-}2}$=0.74 for test No.2). The stiffness improvement ratio (k_s) decreases due to the increase
381 in pre-strengthening tunnel deformation. This means that the postponement of strengthening will
382 cause a decrease in the tunnel stiffness after strengthening. This is because as the tunnel
383 deformation before strengthening increases, the original tunnel stiffness decreases. The structural
384 stiffness of the retrofitted lining depends on both the original segmental lining and the steel plates.

385 Thus, a reduction in segmental lining stiffness due to the delay of strengthening will certainly result
386 in a decrease in the strengthened tunnel stiffness, which appears as a drop of k_s.
387 In order to compare the improvement in total capacity of the tunnel lining due to strengthening at
388 different points, the surcharge level values at the strengthening failure point in each test have been
389 extracted and denoted as SL_f. As seen in Fig.20, the total capacity of the tunnel lining in test No.4
390 is $SL_{f\text{-}4}$=0.44 ($SL_{f\text{-}3}$=0.78 in test No.3, $SL_{f\text{-}2}$=0.91 in test No.2). The total surcharge that can be
391 applied rises, since the strengthening point is postponed. This means that some allowance of tunnel
392 deformation before strengthening can achieve a higher total capacity of the tunnel support after
393 strengthening. Therefore, a sufficient use of the original lining capacity before strengthening
394 benefits the tunnel from the perspective of the total capacity. In practice, it is inappropriate to apply
395 the steel plate strengthening too early to the segmental lining with relatively small deformation.
396 In addition, the increased capacity due to strengthening (denoted as Δ_{SL}) is calculated by the
397 following equation:
398 $$\Delta_{SL} = SL_f - SL_s \quad (4)$$
399 Where SL_s and SL_f are the surcharge levels at the strengthening point and at the strengthening
400 failure point respectively.
401 As illustrated in Fig.20, the increased capacity of the tunnel after strengthening in test No.4 is $\Delta_{SL\text{-}4}$
402 =0.421 ($\Delta_{SL\text{-}3}$=0.442 in test No.3, $\Delta_{SL\text{-}2}$=0.439 in test No.2). It can be seen that there is only a small
403 variance in the increased capacity values, despite the difference in the strengthening point. This
404 means that the improvement in the tunnel bearing capacity after strengthening is not much affected
405 by the variance in the tunnel deformation before strengthening.
406 After strengthening, the retrofitted tunnel behaves as a composite lining composed of the external

original segmental linings and the internal steel plates. The interface between the two components plays a key role. In this experiment, the strengthening failure occurred in the form of interface debonding. The increased capacity of the tunnel after strengthening is related to the interface property, which was kept unchanged in the series of tests in this study. Thus, further research could be conducted to investigate the influence of different interface properties on the segmental tunnel linings strengthened by steel plates.

5. Conclusions

In this paper, a 1-g physical model test was designed and performed to investigate the effectiveness of using steel plates to strengthen the over-deformed segmental tunnel linings. A series of tests were performed for the tunnel without strengthening and for the tunnels being strengthened at different degrees of deformation. The performance was analysed based on data for both the tunnels with and without steel plates strengthening. Some conclusions can be drown from these tests as follows:

(1) Segmental tunnel linings affected by ground surface surcharge deform nonlinearly. As the applied surcharge increases, the joints open and eventually the concrete crushes and lining cracks at the tunnel invert, which leads to a gradual degradation of tunnel lining performance.

(2) Compared with the tunnel without strengthening, the structural performance of the damaged segmental tunnel linings are significantly enhanced with steel plates strengthening. For example, comparing between the results from Test No. 1 (no strengthening) and No. 2 (strengthened tunnel), the stiffness and capacity of the tunnel was improved by 190% and 69%, respectively, due to the steel plate strengthening.

(3) An increase in the tunnel deformation before strengthening (i.e., postponement of strengthening) will result in a decrease in the stiffness and an increase in the total capacity of the tunnel after strengthening, while the increased capacity will be less affected.

Acknowledgement

This study is supported by the Chinese National Science Foundation Committee Program (No. 51538009, No.51978516), and Key Innovation Team Program of Innovation Talents Promotion Plan by MOST of China (No. 2016RA4059). In addition, the author want to show great thanks to Mr. Chen Kun and Ms. Chen Weiyu, who were undergraduate students in Tongji University during the Lab time, for their contributive effort in the experiment process.

Reference

Chang, C.T., Sun, C.W., Duann, S. & Hwang, R.N. 2001a. Response of a Taipei Rapid Transit System (TRTS) tunnel to adjacent excavation. Tunnelling and Underground Space Technology, 16**,** 151-158.

Chang, C.T., Wang, M.J., Chang, C.T. & Sun, C.W. 2001b. Repair of displaced shield tunnel of the Taipei rapid transit system. Tunnelling and Underground Space Technology, 16**,** 167-173.

Chapman, D.N., Ahn, S.K., Hunt, D.V.L. & Chan, A.H.C. 2006. The use of model tests to investigate the ground displacements associated with multiple tunnel construction in soil. Tunnelling and Underground Space Technology, 21**,** 413.

Do, N.A., Dias, D., Oreste, P. & Djeran Maigre, I. 2013. 2D numerical investigation of segmental tunnel lining behavior. Tunnelling and Underground Space Technology, 37**,** 115-127.

Harris, H.G. & Sabnis, G.M. 1999. Structural modeling and experimental techniques, CRC press.

Huang, H.W., Xu, L., Yan, J.L. & Yu, Z.K. 2006. Study on transverse effective rigidity ratio of shield tunnels. Chinese Journal of Geotechnical Engineering, 1, 11-18

Huang, H., Shao, H., Zhang, D. & Wang, F. 2016. Deformational responses of operated shield tunnel to extreme surcharge: a case study. Structure and Infrastructure Engineering, 13**,** 345-360.

Kiani, M., Akhlaghi, T. & Ghalandarzadeh, A. 2016. Experimental modeling of segmental shallow tunnels in alluvial affected by normal faults. Tunnelling and Underground Space Technology, 51**,** 108-119.

Kiriyama, K., Kakizaki, M., Takabayashi, T., Hirosawa, N., Takeuchi, T., Hajohta, H., Yano, Y. & Imafuku, K. 2005. Structure and construction examples of tunnel reinforcement method using thin steel

458 panels. Nippon Steel Technical Report, 92, 45-50.
459 Kojima, Y. & Yashiro, K. 2005. Deformation behavior of tunnel lining due to ground surface loading and
460 unloading above the tunnel. Quarterly Report of RTRI, 46, 143-146.
461 Koyama, Y. 2003. Present status and technology of shield tunneling method in Japan. Tunnelling and
462 Underground Space Technology, 18, 145-159.
463 Lee, K.M. & Ge, X.W. 2001. The equivalence of a jointed shield-driven tunnel lining to a continuous ring
464 structure. Canadian Geotechnical Journal, 38, 461-483.
465 Liu, X., Jiang, Z., Yuan, Y. & Mang, H.A. 2017. Experimental investigation of the ultimate bearing
466 capacity of deformed segmental tunnel linings strengthened by epoxy-bonded steel plates.
467 Structure and Infrastructure Engineering, 14, 685-700.
468 Mair, R., Taylor, R. & Bracegirdle, A. 1993. Subsurface settlement profiles above tunnels in clays.
469 Geotechnique, 43.
470 Meguid, M.A., Saada, O., Nunes, M.A. & Mattar, J. 2008. Physical modeling of tunnels in soft ground: A
471 review. Tunnelling and Underground Space Technology, 23, 185-198.
472 RAIB 2014. Rail Accident Report: Penetration and obstruction of a tunnel between Old Street and Essex
473 Road stations, London 8 March 2013. Derby, UK: Rail Accident Investigation Branch,
474 Department for Transport.
475 Shao, H., Huang, H., Zhang, D. & Wang, R. 2016. Case study on repair work for excessively deformed
476 shield tunnel under accidental surface surcharge in soft clay. Chinese Journal of Geotechnical
477 Engineering, 38, 1036-1043.
478 Standing, J.R. & Lau, C. 2017. Small-scale model for investigating tunnel lining deformations. Tunnelling
479 and Underground Space Technology, 68, 130-141.
480 Van Empel, W., Sip, J. & Haring, F. 2006. Design of repair measures of a damaged shield driven tunnel.
481 Tunnelling and Underground Space Technology, 21.
482 Wang, S., Jian, Y., Lu, X., Ruan, L., Dong, W. & Feng, K. 2019a. Study on load distribution characteristics
483 of secondary lining of shield under different construction time. Tunnelling and Underground
484 Space Technology, 89, 25-37.
485 Wang, S., Ruan, L., Shen, X. & Dong, W. 2019b. Investigation of the mechanical properties of double
486 lining structure of shield tunnel with different joint surface. Tunnelling and Underground Space
487 Technology, 90, 404-419.
488 Wood, D.M. 2014. Geotechnical modelling, CRC press.
489 Ye, F., Gou, C.F., Sun, H.D., Liu, Y.P., Xia, Y.X. & Zhou, Z. 2014. Model test study on effective ratio of
490 segment transverse bending rigidity of shield tunnel. Tunnelling and Underground Space
491 Technology, 41, 193-205.
492 Zhang, D.M., Huang, H.W., Hu, Q.F. & Jiang, F. 2015. Influence of multi-layered soil formation on shield
493 tunnel lining behavior. Tunnelling and Underground Space Technology, 47, 123-135.
494 Zhang, D.M., Zhai, W.Z., Huang, H.W. & Chapman, D. 2019a. Robust retrofitting design for rehabilitation
495 of segmental tunnel linings: Using the example of steel plates. Tunnelling and Underground
496 Space Technology, 83, 231-242.
497 Zhang, D.M., Zhang, D.M., Soga, K., Huang, H.W. & Wang, F. 2019b. Rehabilitation of Overdeformed
498 Metro Tunnel in Shanghai by Multiple Repair Measures. Journal of Geotechnical and
499 Geoenvironmental Engineering, 145, 04019101.
500 Zhao, H., Liu, X., Bao, Y., Yuan, Y. & Bai, Y. 2016. Simplified nonlinear simulation of shield tunnel lining
501 reinforced by epoxy bonded steel plates. Tunnelling and Underground Space Technology, 51,

362-371.
Zheng, G., Cui, T., Cheng, X., Diao, Y., Zhang, T., Sun, J. & Ge, L. 2017. Study of the collapse mechanism of shield tunnels due to the failure of segments in sandy ground. Engineering Failure Analysis, 79**,** 464-490.

507 **Table 1.** Scale Factors adopted in 1-g model test

Quantity	Symbol	General	Scaling ratio
Length	l	n_l	1:15
Unit weight	γ	n_γ	1:1
Elastic modulus	E	$n_E=n_l\times n_\gamma$	1:15
Pressure	q	$n_q=n_l\times n_\gamma$	1:15
Strain	σ	$n_\sigma=n_L\times n_\gamma$	1:15
Displacement	δ	$n_\delta=n_l$	1:15
Strain	ε	n_ε	1:1
Force	F	$n_F=n_l^3\times n_\gamma$	$1:15^3$
Moment	M	$n_M=n_l^4\times n_\gamma$	$1:15^4$
Flexural rigidity	EI	$n_{EI}=n_E\times n_l^4$	$1:15^5$

508

509

510 **Table 2.** Properties of the model soil materials

Parameters	Unit	Symbol	Rubber particles	Dry sand
Unit weight	kN/m^3	γ	8.6	15.6
Water content	%	w	0	0
Medium grain size	mm	d_{50}	3	0.32
Uniformity coefficient	-	C_u	1.9	3.3
Compression modulus	MPa	E_s	0.51	18.18
Friction angle	°	φ	31.5	33.1

511

512

513 **Table 3.** tunnel model dimensions

Quantity	Symbol	Unit	Model	Prototype	Scaled ratio
Outer diameter	D	mm	410	6150	1:15
Lining thickness	t	mm	25	375	1:15
Embedded wire diameter	ϕ	mm	1.6	-	-

514 **Table 4.** Properties of the gypsum used for tunnel model manufacture

Quantity	Symbol	Unit	Model	Prototype	Actual scaled ratio
Compressive strength	σ_g	MPa	2.23	32.4	1:14.5
Elastic modulus	E_g	GPa	1.89	34.5	1:18.2

515

516

517 **Table 3.** A series of tests for tunnels strengthened at different degrees of damage

Test No.	p1 (kN)	Steel plate strengthening
1	-	No
2	6	Yes
3	4	Yes
4	0	Yes

518

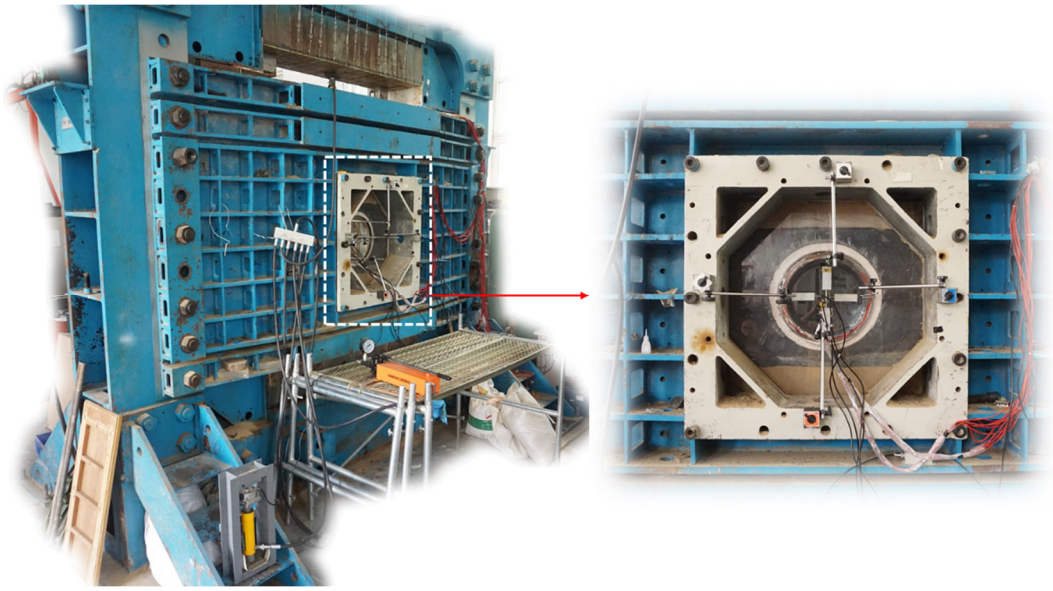

(a) (b)

Figure 1 Photographs of the experiment apparatus, (a) an overview, (b) a view of the tunnel

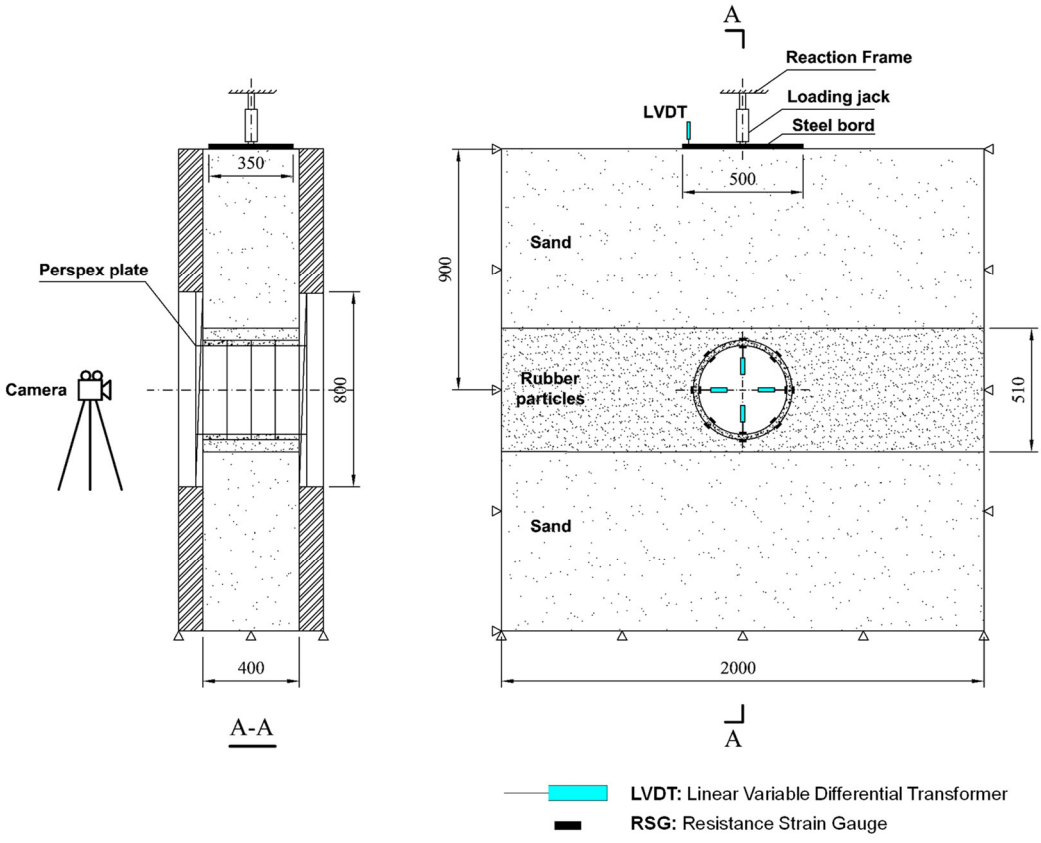

Figure 2 A diagram showing the experimental apparatus (unit: mm)

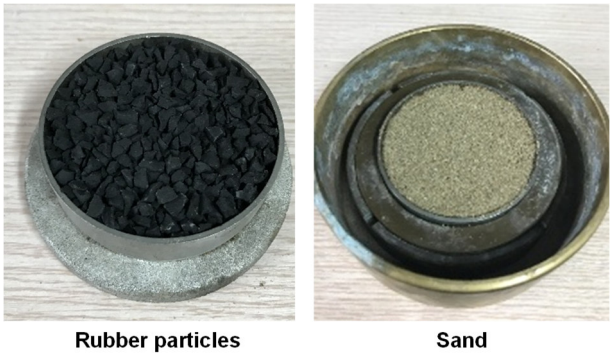

Figure 3 Rubber particles and a sand sample

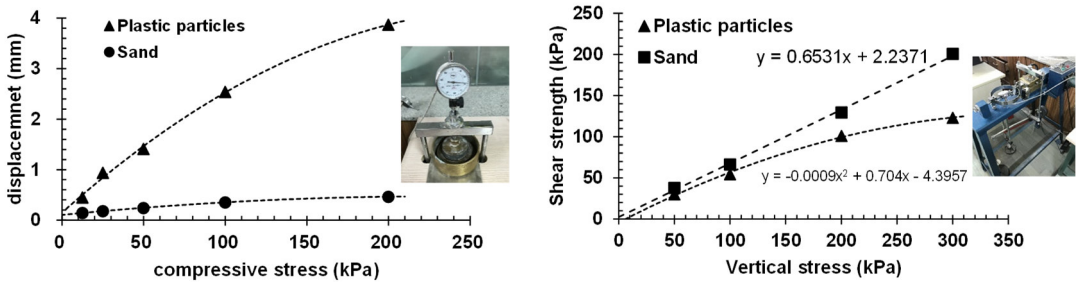

(a) (b)

Figure 4 Test results for the model soil materials, (a) compressibility test results, (b) direct shear test results

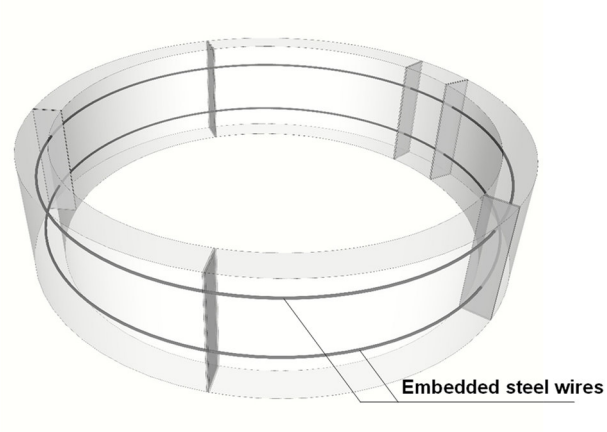

Figure 5 A diagram showing the arrangement using to model the segmental tunnel lining

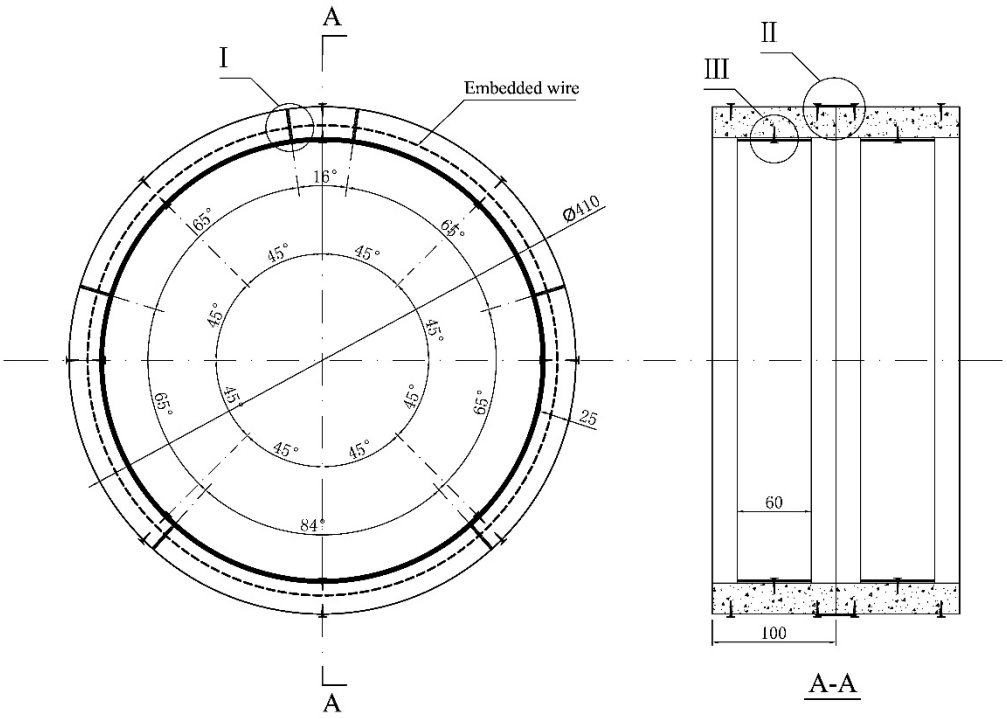

(a)

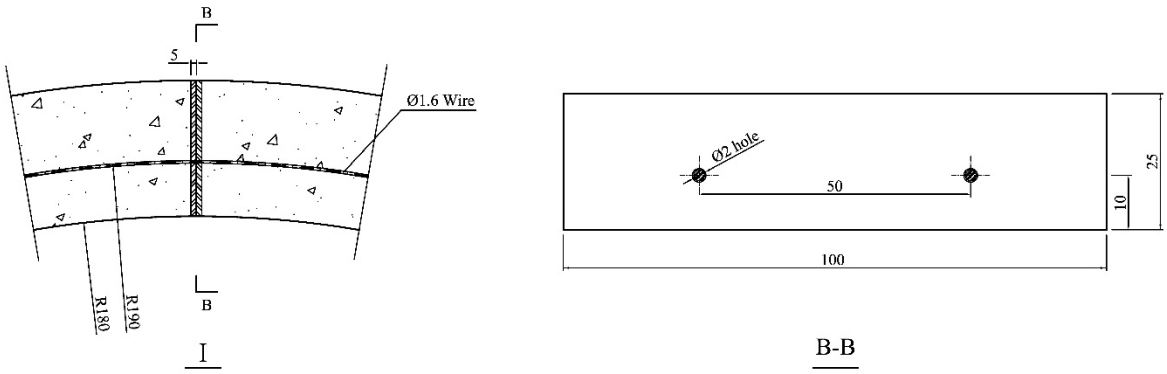

(b)

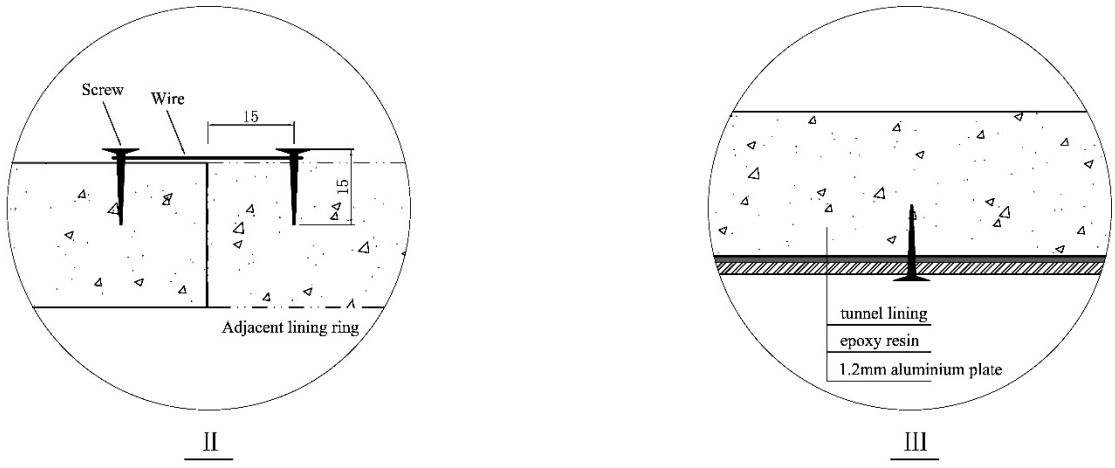

(c) (d)

Figure 6 Detailed drawings of the segmental tunnel lining model (unit: mm), (a) An overall drawing

of the segmental lining ring and screws arrangement, (b) A detailed drawing of the segmental joint, (c) The connection between adjacent lining rings, (d) The interface between the lining and the steel plate.

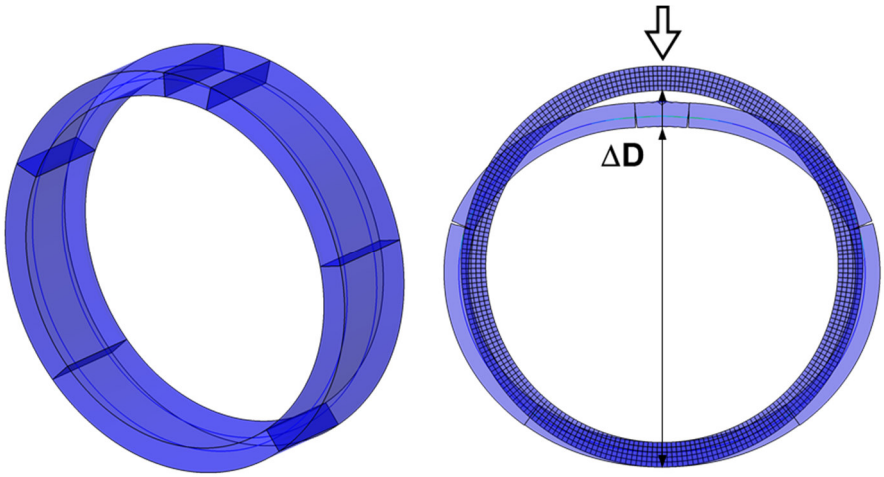

(a) (b)

Figure 7 Numerical simulation for tunnel model design (a) the finite element model (b) the numerical test for evaluating the effective ratio of the transverse bending rigidity.

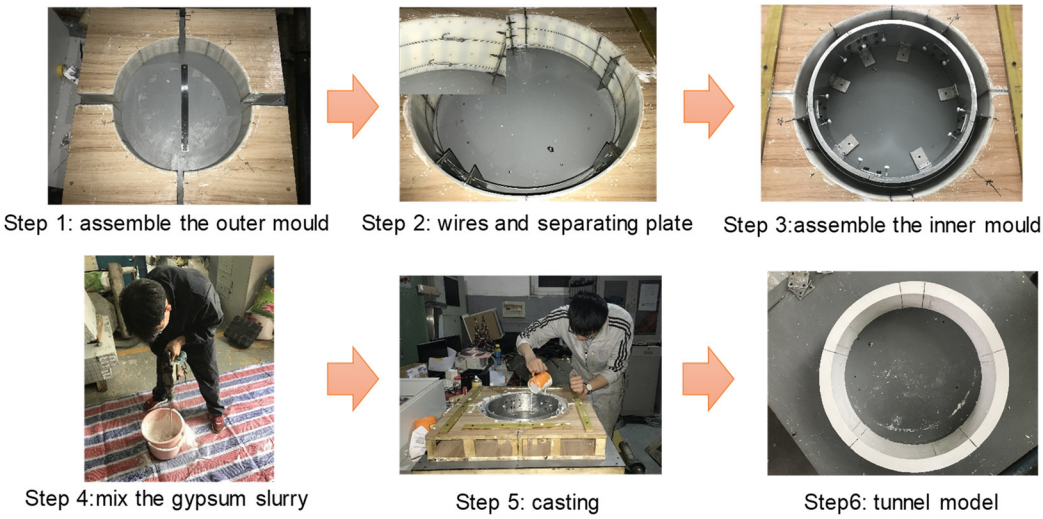

Figure 8 Manufacturing process for the model segmental tunnel linings

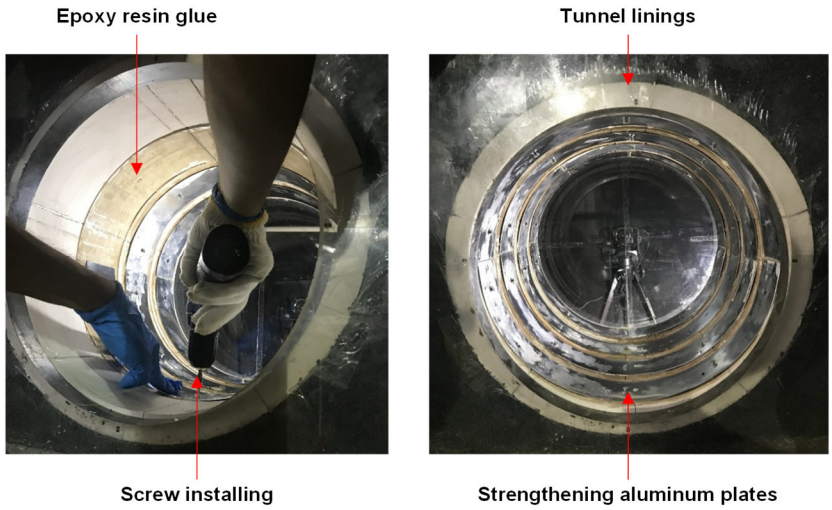

(a) (b)

Figure 9 modelling the steel plate strengthening for existing segmental tunnel linings using aluminum steel plates (a) Installing the aluminum plates (b) The final strengthened tunnel

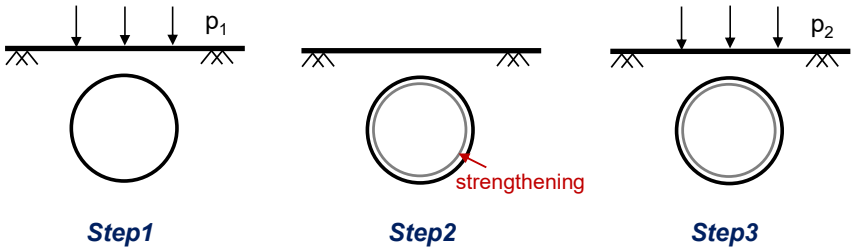

Figure 10 Test procedure for the steel plates strengthened segmental tunnel linings

(a) (b)

Figure 11 Photographs of the tunnel without strengthening (a) the initial tunnel profile; (b) the damaged tunnel profile

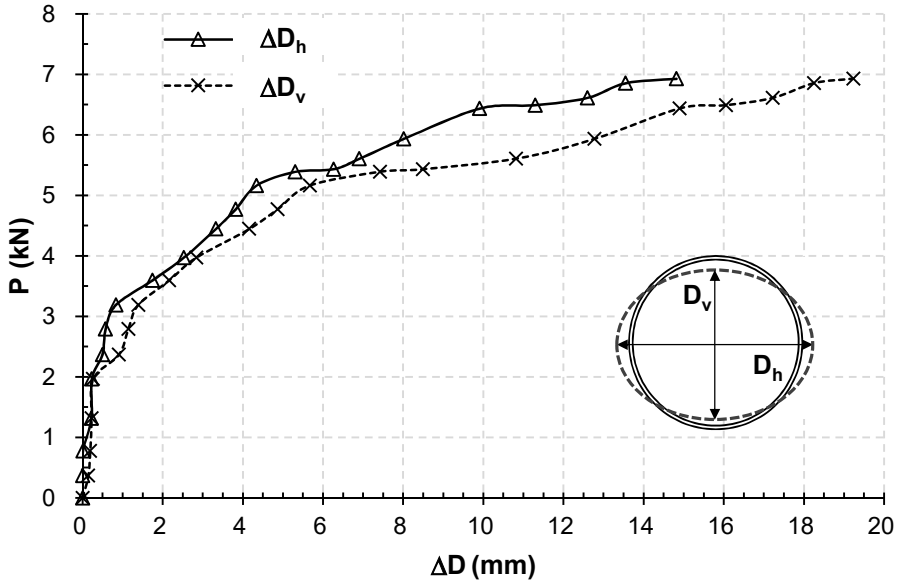

Figure 12 Tunnel cross-section deformation in terms of changes in horizontal and vertical diameters

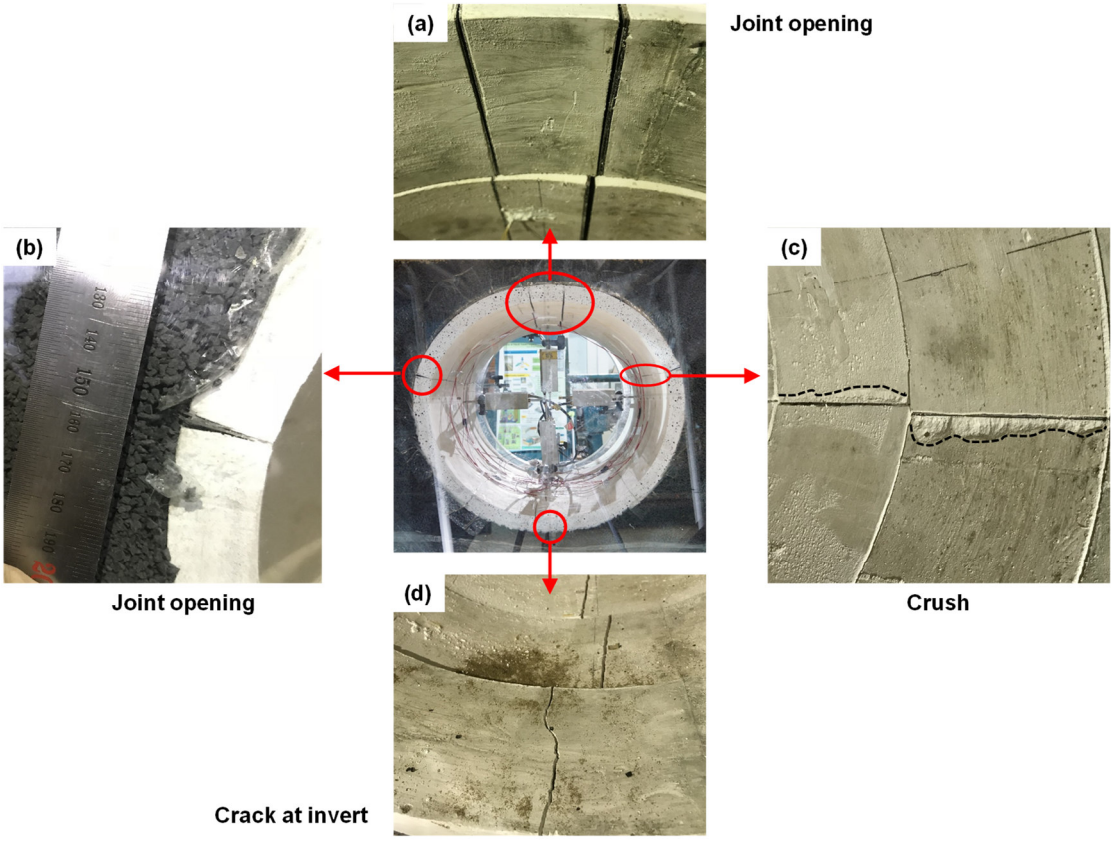

Figure 13 Details of the defects in the damaged segmental tunnel linings

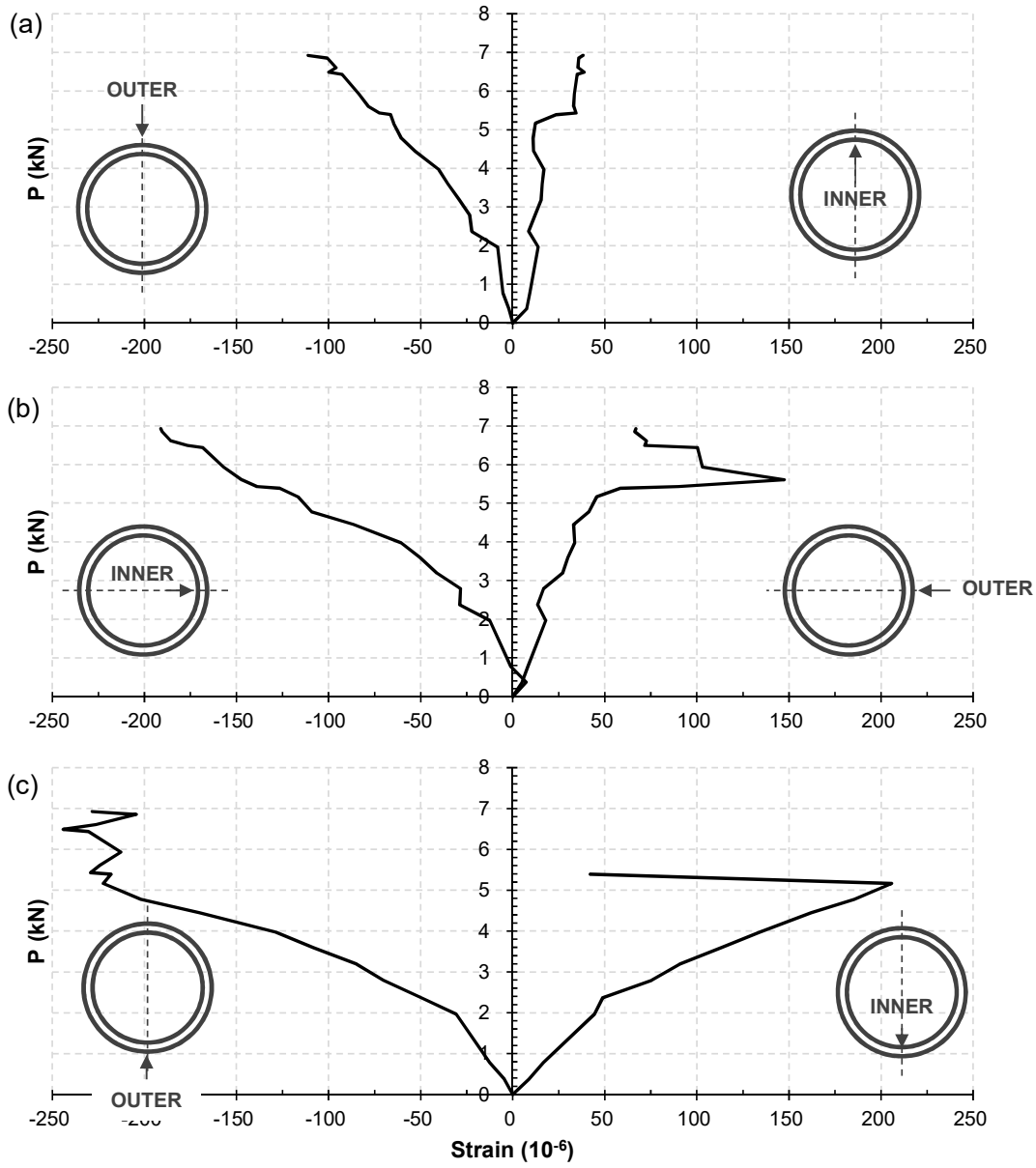

Figure 14 Strain measurements of lining segments at different locations, (a) crown (b) spring-line (c) invert

(a) (b)

Figure 15 Photographs of tunnels strengthened with aluminum plates, (a) after strengthening (b) after the occurrence of strengthening failure

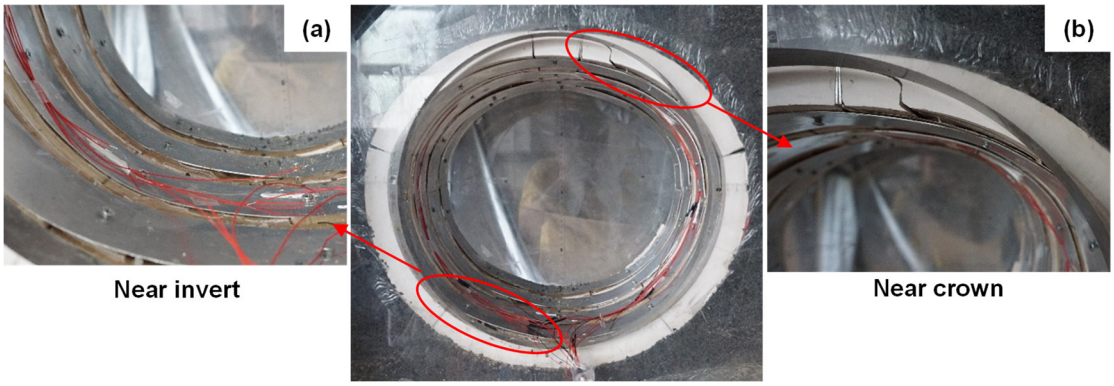

Figure 16 Detailed features of the debonding failure of the strengthened segmental linings, (a) the interface near the tunnel invert, (b) the interface near the tunnel crown

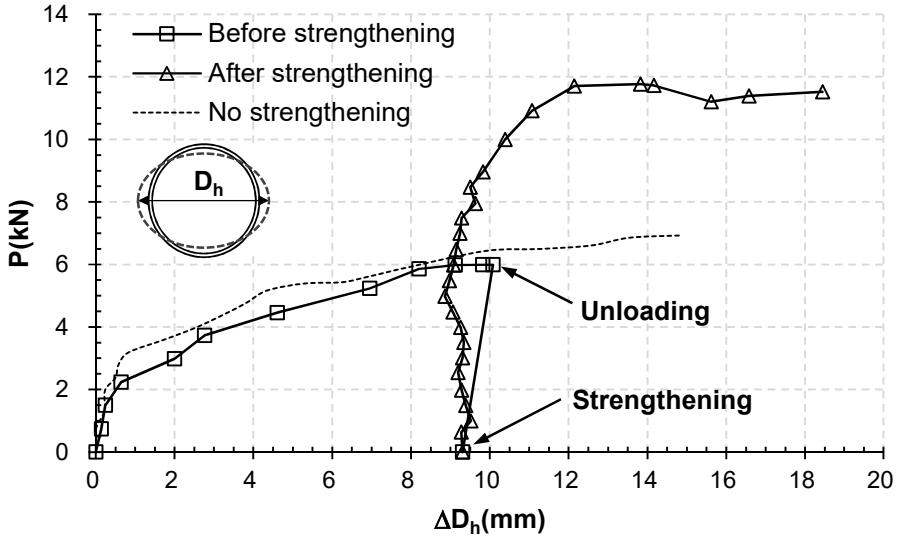

(a)

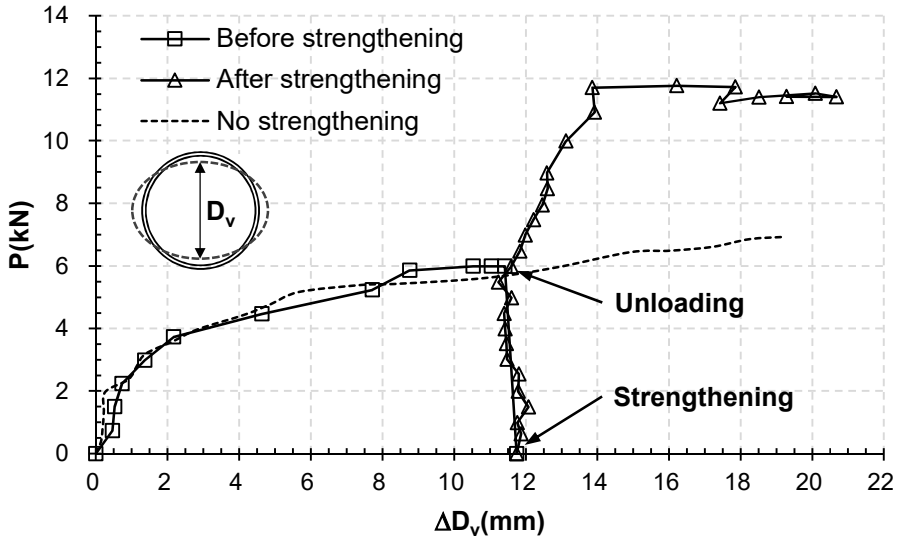

(b)

Figure 17 *P-ΔD* curves for the tunnel strengthened by steel plates, (a) horizontal deformation *P-ΔD*$_h$ (b) vertial deformation *P-ΔD*$_v$

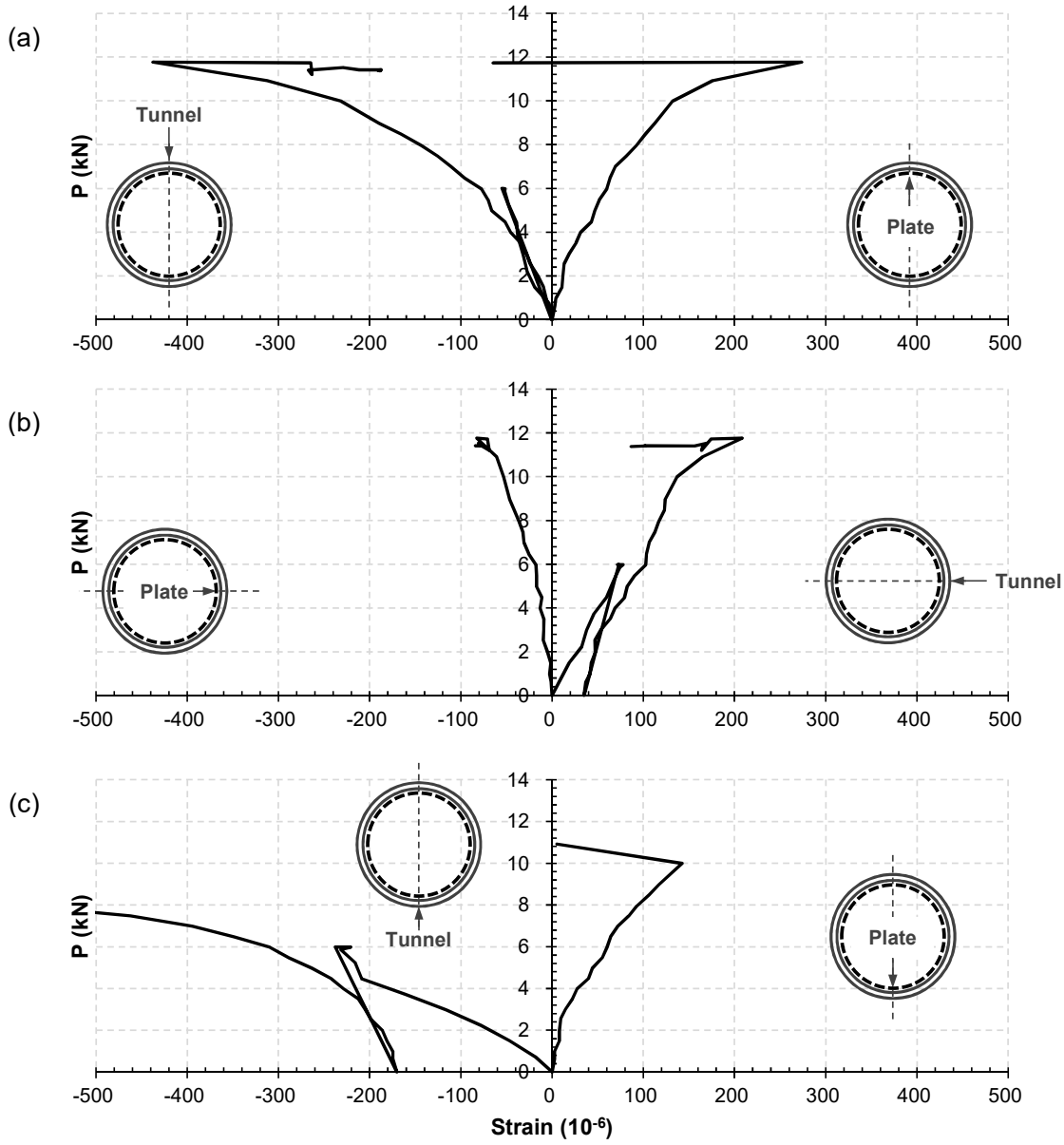

Figure 18 Strain values at the outer edge of the tunnel lining and the steel plate at different positions, (a) crown, (b) spring-line, (c) invert

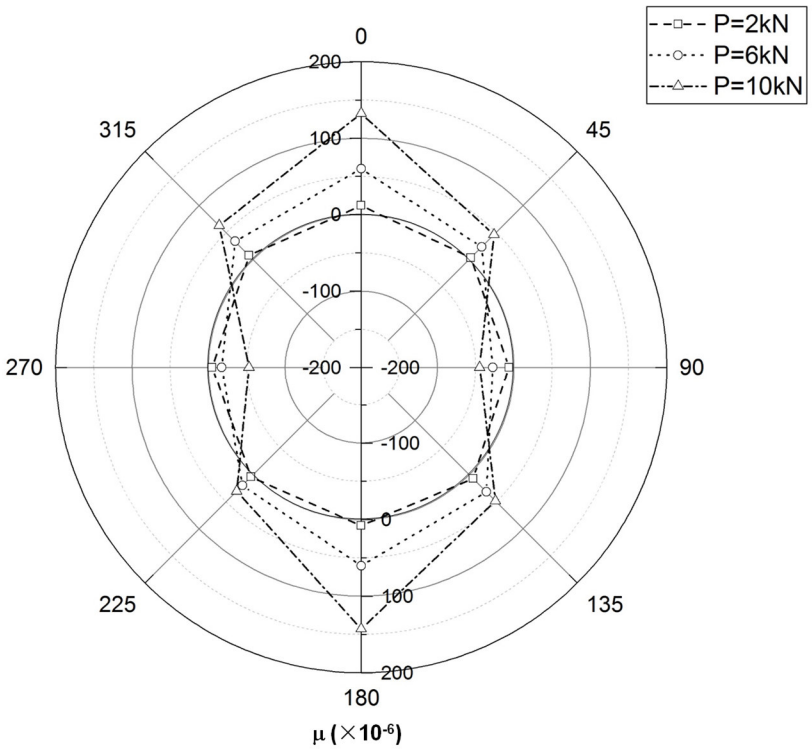

Figure 19 Strain distribution in the strengthening steel plate at different loading stages

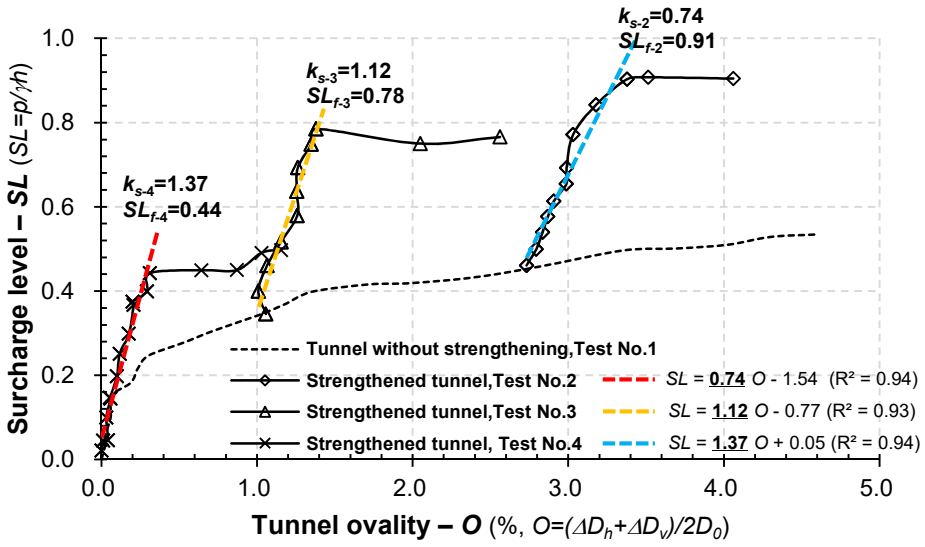

Figure 20 The relationship between the surcharge level and the ovality of the tunnels being strengthened at different degrees of damage